

OMAE2009-80002

Numerical simulations of cylinder VIV focusing on high harmonics

Yiannis Constantinides
Chevron Energy Technology Company

Owen H. Oakley, Jr.
Chevron Energy Technology Company

ABSTRACT

The discovery of high frequency contributions in flexible cylinder VIV during the DeepStar experiments revealed a significant omission and raised concerns among riser designers due to the high fatigue contribution. Researchers are now focusing on this area by analyzing the sparse experimental data or performing simplified experiments. Building on past success with CFD simulations, this numerical study focuses on understanding the origin and cause of the 3rd harmonic in particular. An array of basic spring supported rigid cylinder and various configurations of flexible cylinder computations are performed to validate CFD and to gain a qualitative understanding. A relationship between the hydrodynamic force causing the 3rd harmonic and cylinder motion as well its spatial characteristics is established.

instrumentation limitations. High L/D risers generally experience VIV excitation over a limited region and have large damping, or power-out, regions. End reflections and unsteadiness introduce further complications making the interpretation of point measurements challenging. Very different things are happening in time and in space. We would therefore like to better understand the nature of marine riser motions. In the absence of densely instrumented full scale riser data, CFD modeling of high L/D flexible cylinders offers the possibility of improved insight.

This paper first discusses the source of the harmonic content from the viewpoint of rigid cylinder motions and the connection with inline motions. The subject is then expanded to include spatial effects for high L/D flexible cylinders.

INTRODUCTION

The presence of higher harmonic content in cylinder vortex induced vibrations has been noted in many experimental investigations over the years [1-4]. It has received relatively little notice because it is barely visible in the motions and is only obvious in the force or acceleration signals. Also many of the experiments were rigid 1-dof cylinders. This configuration suppresses the in-line motion and the harmonics, as will be made clear below. The higher harmonic content of 2-dof VIV could have a major impact on the amount of curvature/strain and number of cycles, greatly increasing the fatigue damage over the fundamental Strouhal excitation frequency. Significant harmonic content in strain was observed in the DeepStar flexible cylinder experiments [1,3]. The lack of such harmonics in reports of full scale riser measurements in some cases could be due to

LIFT FORCE DESCRIPTION AND MOTION RELATION

It is often difficult to understand the structural and fluid dynamics of flexible cylinder VIV due to the complexity of the two areas and the coupling in between them. A typical first approach is to simplify the problem looking at a reduced order structural model and a shorter fluid domain to gain a basic understanding. Therefore, we designed a numerical experiment utilizing a free moving rigid cylinder in an effort to understand the hydrodynamic forces causing the high harmonics over a shorter riser section. The CFD model consisted of a spring supported circular cylinder configuration that could undergo VIV at supercritical Reynolds numbers. A fine mesh of $\sim 7M$ elements was utilized to obtain a DES solution for the 3 diameter span of the cylinder simulated. Initially a validation was performed against relevant experiments for 1-DOF and 2-DOF ($k_{IL}=4k_{CF}$) motion

showing a good agreement between CFD and experiments (Table 1).

Case	CFD	Experiment
1-DOF $V_{rn}=6.0$	$A^*_{CF}=0.78$	$A^*_{CF}=0.8$
2-DOF $V_{rn}=7.4$	$A^*_{CF}=0.87,$ $A^*_{IL}=0.44$	$A^*_{CF}=0.8,$ $A^*_{IL}=0.4+$

Table 1 Comparison of crossflow and inline motions for 1-DOF and 2-DOF cases.

The crossflow force and motion of the 1-DOF case are presented in Figure 1, showing the typical VIV behavior of the motion being synchronized with the force at the same frequency. The introduction of the inline motion, in the 2-DOF case, made a dramatic change in the crossflow force as it can be seen in Figure 2. Although the cylinder vibrates at the same frequency (1x) and similar amplitude, the driving force is primarily at 3x the motion frequency. Closer inspection of the motion reveals a small 3x motion with a high acceleration due to the 3x oscillation frequency. The force also consists of a weaker 1x component in addition to the dominant 3x at this reduced velocity ($V_{rn}=7.4$).

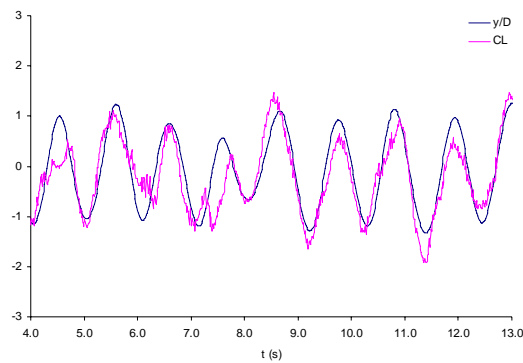


Figure 1 Crossflow motion and force for a 1DOF rigid cylinder motion.

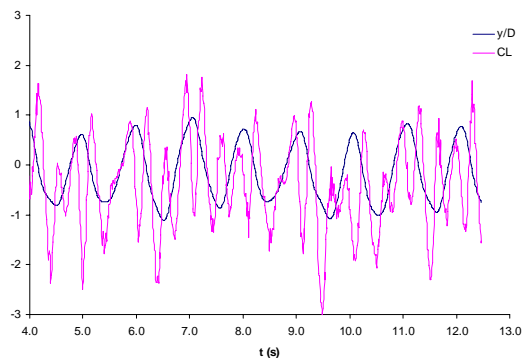


Figure 2 Crossflow motion and force for a 2DOF rigid cylinder motion showing strong 3rd harmonic content.

The cylinder trajectory and force, presented in Figure 3, reveal a pattern between cylinder location and force peak values (maximum and minimum). At the start of the trajectory, the

cylinder is located near the center, moving downstream. Just before it reaches the maximum crossflow offset, it starts to move upstream and sheds a vortex. At this point the crossflow force peaks to a maximum at point 4. With the cylinder moving upstream, another vortex is shed at 5 as it starts to move downstream. The force assumes to a minimum. The next force peak is when the cylinder passes through the center, at point 6, and it is a maximum. The increase in force may not be entirely due to a new vortex shed but also due to the location relative to the vortex field. The same process is repeated over the other symmetric part of the cycle leading to a dominant 3x force field per motion cycle with secondary 1x components and traces of 5x at this reduced velocity. The odd harmonics (i.e. 1x, 3x, 5x) are symmetric with respect to the crossflow motion. This may also explain the absence of the even harmonics that would introduce asymmetry in the motion that is physically expected to be symmetric. The sign of the peak forces over the other half of the cycle is reversed as the vorticity of the system has an opposite sign. In the 1-DOF case the force peaks only at the maximum crossflow offset points leading to the typical 1x force field.

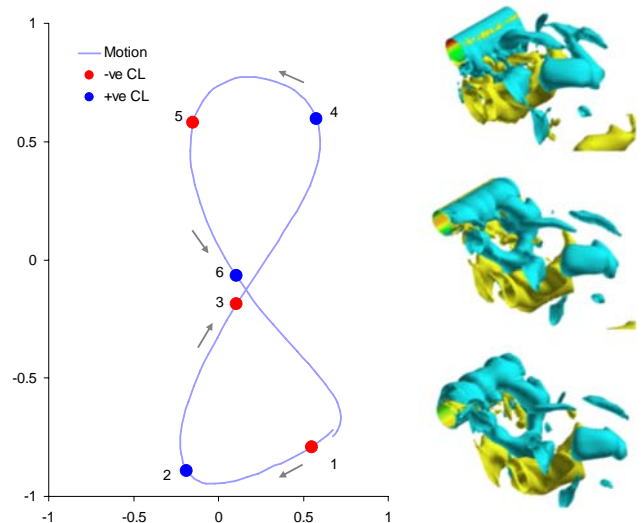


Figure 3 Trajectory and peak crossflow forces in a 2DOF rigid cylinder motion with high 3rd harmonic and flow visuals of vorticity at instances 4, 5 and 6 (from top to bottom).

The study of the force motion relation revealed that the inline motion was the key to generating the 3x forces. A set of runs was subsequently devised to capture the relation of force and motion. To capture part of the response surface for a given reduced velocity, the inline and crossflow motion was varied. This was achieved by introducing damping to the system while retaining the same spring constants and V_{rn} producing 3 basic sets of runs:

- Inline only damping
- Crossflow only damping
- Inline and crossflow damping

A total of 28 runs were completed using different damping values for each of the three sets. The force signal was processed to extract the harmonic contributions through filtering. In particular, we are interested in the 3x harmonic, shown in Figure 4 for $V_{rn}=7.4$, as a function of the inline and crossflow motion amplitudes. The plot shows a clear relation between the crossflow 3x force and inline motion but none with the crossflow motion as one would initially suspect. Remarkably, the 3x crossflow force varies linearly with the inline motion as shown in Figure 5, for the current V_{rn} . This correlates well with the explanation of the mechanism given in the previous paragraph and also explains why the 1-DOF configuration does not contain high harmonics. For a full mapping of the response field a prescribed motion study is required expanding the computations to include various V_{rn} and phase differences between inline a crossflow.

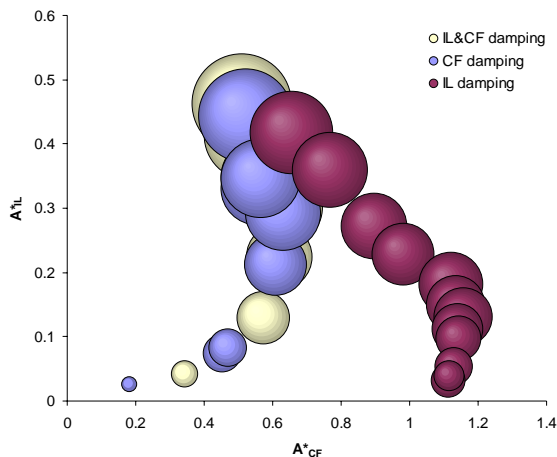


Figure 4 Third harmonic rms crossflow force as a function of inline and crossflow nominal motions. Bubble size proportional to 3x crossflow force.

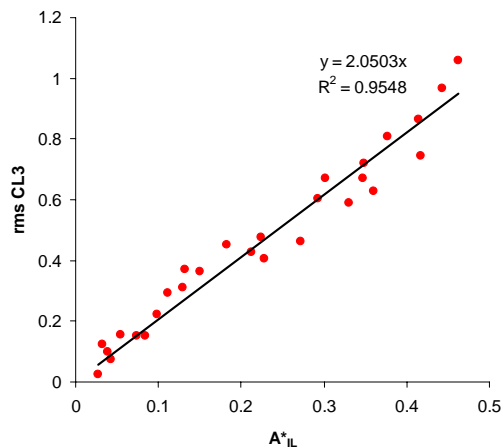


Figure 5 Third harmonic rms lift force as a function of inline motion for $V_{rn}=7.4$.

VERIFICATION OF INLINE MOTION EFFECT ON HIGH HARMONICS

To verify whether the findings of the short cylinder section experiments apply to flexible cylinders, a set of computations were conducted on a flexible cylinder configuration to introduce a more representative structural model and a longer aspect ratio. The setup consisted of a 500 L/D tension dominated flexible cylinder responding to mode 3 crossflow and 6 inline. A set of cases were designed to investigate the effect of inline motion and the importance of inline modes on high harmonics. This was accomplished by excluding structural modes from the flexible cylinder structural model. The cases shown in Table 2 verify that in the absence of inline motion (case 2) there are no harmonics in the acceleration spectrum. Also when the 2x inline modes are restricted (case 4) the high harmonics are suppressed despite the fact that the 1x modes are available. When 1x modes are restricted (case 3), and 2x are available, the high harmonics are present. The study clearly suggests that indeed high harmonics are caused by the inline motions and more specifically by the 2x inline modes.

Case	IL modes allowed	CF modes allowed	High Harmonics
1	All	All	Yes
2	None	All	No
3	2x only	All	Yes
4	1x only	All	No

Table 2 Loadcases and results for the flexible cylinder study responding at mode 3 crossflow (referred as 1x mode).

SPATIAL DISTRIBUTION ON HIGH ASPECT RATIO CYLINDERS

As a natural progression to understand the high harmonics, a more realistic simulation of a deepwater riser was utilized to validate CFD and to understand the spatial distribution of forces and strains. A high aspect ratio ($L/D=4137$) tension dominated system was simulated in sheared currents environments at subcritical Reynolds numbers. The modeling methodology and further details can be found in [7].

First we present the comparison between the simulations and experiments for the given case in [3]. The total strain and harmonic components are in good agreement with the experiment (Figure 6). Further the response character is remarkably close to the experiment highlighting traveling waves in the center part of the riser and unsteady “standing wave” regions at both ends. These are caused by the reflections of the traveling waves at the boundaries as it can also be seen from Figure 7 over a shorter time window. The

vibrations are generated near the bottom of the riser and travel both upwards and downwards.

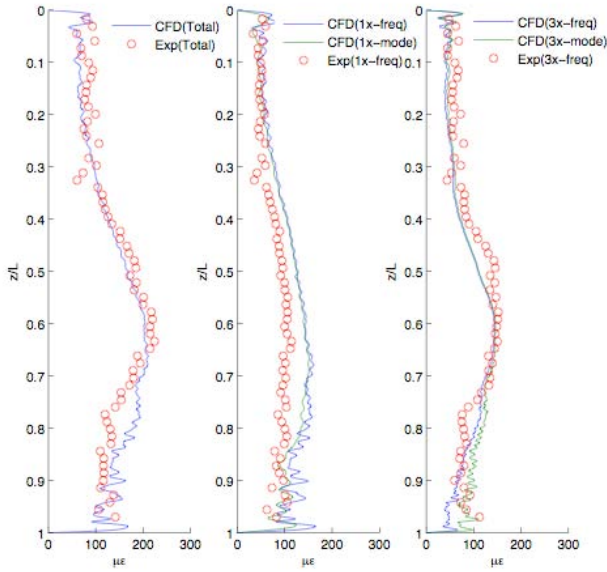


Figure 6 Comparison of CFD predictions with experiments (total strain, 1x and 3x) and comparison between strain content in selected modes vs selected frequency band. Both 1x and 3x strain are primarily caused by resonant modes at resonant frequencies besides small deviations at the ends of the riser where the motion is reflected back causing quasi-steady standing wave type behavior.

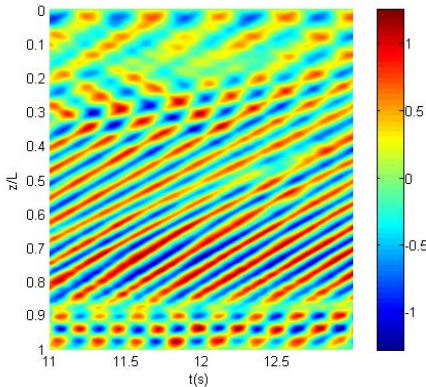


Figure 7 Crossflow motion evolution response along the riser, showing strong traveling wave characteristics generated from the bottom part of the riser where the current speed is higher.

In this study we focus on the data analysis and interpretation of the simulations. The response and hydrodynamic forces were analyzed using spectral analysis and modal decomposition. A zero phase elliptic filter was constructed to filter the signal into components corresponding to the first (1x) and third (3x) harmonic. The signal was also decomposed into

eigenfunctions or modes, assuming simple modes of sinusoidal shape, a reasonable first approach for a tension dominated cable.

$$\hat{y}_{n_y f_y}(z, t) = \sum_{i=n_s}^{n_e} \sin\left(\frac{i\pi z}{L}\right) \hat{W}_i(t)$$

$$\hat{F}_{n_F f_F}(z, t) = \sum_{i=n_s}^{n_e} \sin\left(\frac{i\pi z}{L}\right) \hat{W}_i(t)$$

where, $y(z, t)$ and $F(z, t)$ are the cylinder displacements and hydrodynamic force varying in time and position, $w_i(t)$ the i^{th} modal weight varying with time, n_s and n_e are the starting and ending mode number, $n_y f_y$ and $n_F f_F$ indicate the modal (n) and frequency (f) content. For example y_{13} is the displacement for 1x modal range at the 3x frequency band. As the mode-shapes are not based on the complex formulation it is important to include a range of modes to describe a traveling wave. A single mode will yield a pure standing wave.

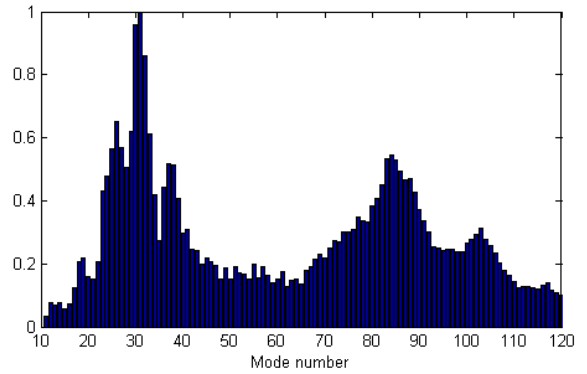


Figure 8 Modal participation of acceleration normalized by peak value. The 1x modal range includes modes 10 through 60 and the 3x modes 61 through 120.

As we are interested in the power in and out of the system and also on the hydrodynamic forces, the lift coefficient in phase with velocity was also calculated [9]. The coefficients were calculated for each harmonic, based on the both the mode number (n) and frequency (f) of the crossflow force (F) and response motion or velocity (y).

$$Cl_{v_{n_F f_F n_y f_y}}(z) = \frac{\frac{2}{T} \lim_{T \rightarrow \infty} \int_t^{t+T} F_{n_F f_F}(z, t) \bullet \dot{y}_{n_y f_y}(z, t) dt}{\frac{1}{2} \rho D L_e U(z)^2 \times \left(\sqrt{2} \text{std}(\dot{y}_{n_y f_y}(z, t)) \right)}$$

In time, the response and location where the traveling waves are generated will shift slightly. This is referred to as mode switching. In this study we analyze the data over a short window in time where the response appears steady and

captures primarily one power in region. The frequency filtered strains and crossflow forces corresponding to 1x and 3x frequency bands indicate a good correlation between them (Figure 9). Both components travel along the riser with the same speed as expected and have similar “traveling” and standing regions, with the 3x component have a wave number three times higher than the 1x frequency. The higher 3x component is phase locked to the 1x component.

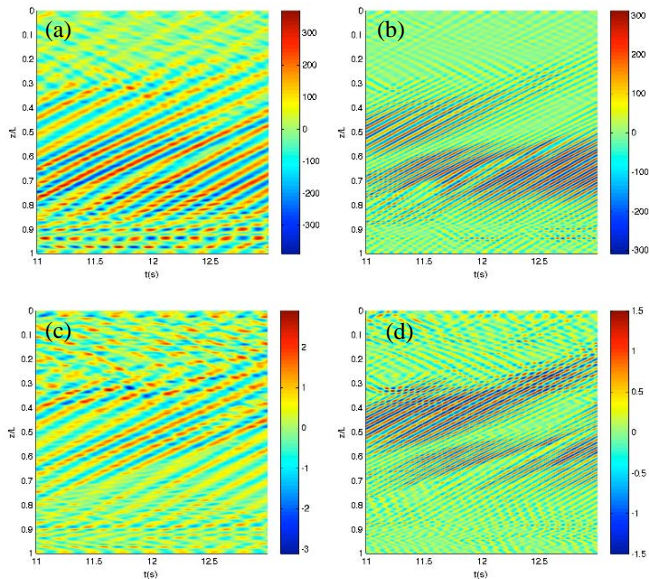


Figure 9 Crossflow microstrain 1x (a), 3x (b) and lift coefficient 1x (c), 3x (d).

The instantaneous force coefficients (CI) values as well as the rms statistics over the selected time interval are presented in Figure 10 and Figure 11, decomposed to modes and frequencies per our methodology. The 1x force primarily consists of 1x modal components at 1x frequency as expected.

We also observed a small rms non-resonant component of the 1x mode at 3x frequency. It is postulated that this is probably caused by the high harmonic force. The 3x mode shows a similar participation of frequencies. It is dominated by 3x frequency force and a smaller non-resonant force at 1x frequency. The 3x total force closely follows the rms distribution of the 1x along the riser. Overall the 3x strain is caused by the corresponding force at 3x frequency and mode.

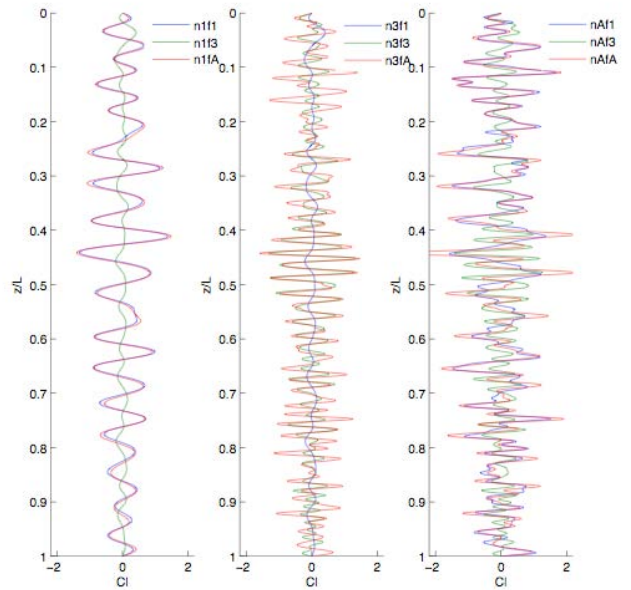


Figure 10 Instantaneous lift coefficient CI decomposed into modes and frequencies. Left is the 1x mode components of the 1x frequency (n1f1) 3x frequency (n1f3) and all frequencies (n1fA). Center is the 3x mode components and on right all modes.

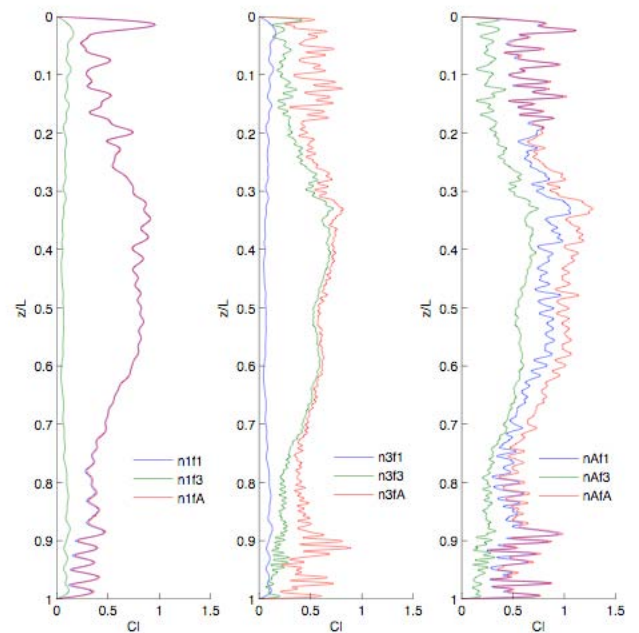


Figure 11 RMS lift coefficient CI decomposed into modes and frequencies. Left is the 1x mode components of the 1x frequency (n1f1) 3x frequency (n1f3) and all frequencies (n1fA). Center is the 3x mode components and on right all modes.

The crossflow force magnitude for the primary harmonic is at the same order values as rigid cylinder experiments and computations. The third harmonic forces extracted in the power in region of 0.7L-0.9L show a linear relationship with the inline motion similar to the short section simulations performed here. It is difficult to compare the short section values to the existing flexible cylinder and draw direct conclusions as they were done at slightly different reduced velocities and Reynolds numbers. Overall they follow the same trend and have values the same order of magnitude. It is postulated that values at a lower V_{rn} and closer to the value of the flexible cylinder power-in will have higher 1x contributions and lower 3x, reaching a better agreement between the two sets.

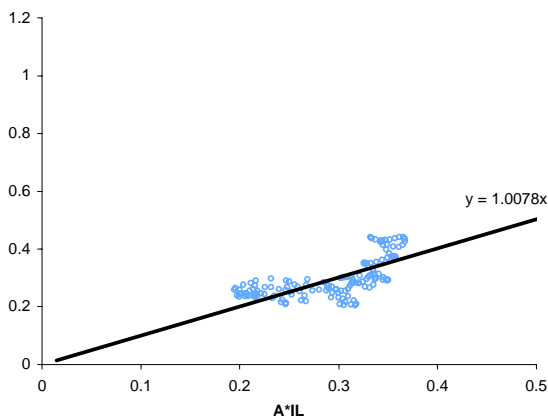


Figure 12 Third harmonic rms lift against nominal inline motion.

The lift coefficient in phase with velocity (Cl_v) was also calculated for the corresponding modes and frequencies; see Figure 13. The primary Cl_v (Cl_{v1111}) shows that the power-in, (positive Cl_v values) is located in the high current area between 0.7L and 0.9L. Negative values indicate that power is extracted from the system as the vibrations travel upwards (power-out regions). At the top end, where the vibrations are reflected back, there is secondary power-in region of a ‘standing wave’ type of character. The frequency associated with the local vibrations is also smaller than the primary regions as it is located in an area with a smaller current and higher inclination. Similarly, at the bottom of the riser we find a secondary power-in region and a ‘standing wave’ type of response. The pure ‘resonant’ 3x coefficient (Cl_{v3333}) follows the same pattern as the primary with similar power in and out regions. Overall the non resonant coefficients (Cl_{v1313} and Cl_{v3131}) appear to be of ‘standing wave’ character especially at the ends of the riser where they have higher values.

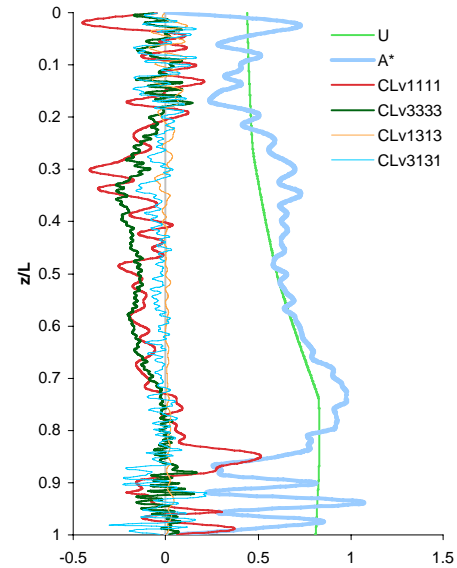


Figure 13 Lift coefficients in phase with velocity for first (Cl_{v1111}) and third harmonic (Cl_{v3333}) as well non-resonant components (Cl_{v1111} : n1f1 force with n1f1 velocity etc).

CONCLUSIONS

A numerical study was performed to gain a basic understanding of the high harmonics, in particular the 3rd crossflow and to validate the CFD model. The study indicates a clear hydrodynamic force at three times the frequency of the classical VIV force, now referred as the first harmonic. The third harmonic is caused by the inline motion of the cylinder and it is linearly proportional to the inline amplitude. On a flexible cylinder, the third harmonic will travel at the same speed as the first harmonic but oscillate at three times the frequency. Although the motion amplitude is very small, the generated strain will be large due to the high curvature. Further, the third harmonic force will have the same spatial distribution as the equivalent motion, causing a response at the same ‘mode’. Analysis of the first harmonic indicates a primary power-in region in the high current area and secondary regions near the ends, corresponding to ‘standing wave’ type areas.

A data extraction methodology was also utilized to extract hydrodynamic coefficients from CFD data. We view the extension of this study to high fidelity computations of realistic systems and conditions coupled with an enhanced data analysis as the way forward to uncover the complexity behind VIV.

NOMENCLATURE

A = motion amplitude [m]

D = riser diameter [m]

L = riser length [m]
 Le = riser local section length [m]
 L/D = Aspect ratio [-]
 A/D = normalized amplitude [-]
 A^* = nominal amplitude [-]
 x, y, z = coordinates [m]
 $U(z)$ = current velocity [m/s]
 $F(z, t)$ = hydrodynamic crossflow or lift force [N]
 $y(z, t)$ = crossflow motion [m]
 Cl = lift coefficient
 Cl_v = lift coefficient in phase with velocity
 $Re = UD/\nu$ = Reynolds number [-]
 ν = kinematic viscosity of fluid [m²/s]
 ρ = density of fluid [kg/m³]
 ε = Strain [-]
 t = time [s]
 n = mode number

[8] Constantinides Y, and Oakley O. H, "Numerical prediction of bare and straked cylinder VIV", OMAE2006-92334, 2006

[9] Wu J, Larsen C. M., and K. E. Kaasen, "A new approach for identification of forces on slender beams subjected to vortex induced vibrations", OMAE2008-57550, 2008

[10] Lucor D. and M. S. Triantafyllou, "Riser Response Analysis by Modal Phase Reconstruction", OMAE2006-92265, 2006

REFERENCES

[1] Vandiver J. K., Swithenbank S. B., Jaiswal V. and Jhingran V., "Fatigue Damage from High Mode Number Vortex- Induced Vibration", OMAE2006-9240, 2006

[2] Vandiver J. K., Swithenbank S. B., Jaiswal V. and Jhingran V., "The Effectiveness of Helical Strakes in the Suppression of High Mode-Number VIV", OTC – 18276 – PP, Offshore Technology Conference, 1-4 May 2006, Houston, Texas, USA.

[3] Jhingran, V. And Vandiver J. K., "Incorporating the higher harmonics in VIV fatigue predictions", OMAE2007-29352, 2007

[4] Marcollo H., Chaurasia H., and J. K. Vandiver, "Phenomena observed in VIV bare riser field tests", OMAE2007-29562, 2007

[5] Holmes, S., Oakley O. H. and Y. Constantinides, "Simulation of Riser VIV Using Fully Three Dimensional CFD Simulations", OMAE2006-92124, 2006

[6] Constantinides, Y., O. H. Oakley and S. Holmes, "CFD High L/D Riser Modeling Study", OMAE2007-29151, 2007

[7] Constantinides, Y., O. H. Oakley, "Numerical prediction of VIV and comparison with field experiments", OMAE2008-57215, 2008